Importance of accurately measuring LDOS maps using scanning tunneling spectroscopy in materials presenting atom-dependent charge order: The case of the correlated Pb/Si(111) single atomic layer

C. Tresca [1] T. Bilgeri,[2] G. Ménard,[2] V. Cherkez [2] R. Federici,[2] D. Longo,[2] M. Hervé,[2] F. Debontridder,[2] P. David,[2]
D. Roditchev,[2,3] G. Profeta,[1,4] T. Cren,[2] M. Calandra,[2,5,*] and C. Brun [2,†]

[1]*CNR-SPIN c/o Dipartimento di Scienze Fisiche e Chimiche,*
Università degli Studi dell'Aquila, Via Vetoio 10, I-67100 L'Aquila, Italy
[2]*Sorbonne Université, CNRS, Institut des Nanosciences de Paris, UMR7588, F-75252 Paris, France*
[3]*Laboratoire de Physique et d'Étude des Matériaux, LPEM-UMR8213/CNRS-ESPCI ParisTech-UPMC,*
10 rue Vauquelin, F-75005 Paris, France
[4]*Dipartimento di Scienze Fisiche e Chimiche, Università degli Studi dell'Aquila, Via Vetoio 10, I-67100 L'Aquila, Italy*
[5]*Dipartimento di Fisica, Università di Trento, via Sommarive 14, I-38123 Povo, Italy*

We address here general issues and show how to properly extract the local charge order in two-dimensional systems from scanning tunneling microscopy/spectroscopy (STM/STS) measurements. When the charge order presents spatial variations at the atomic scale inside the unit cell and is energy dependent, particular care should be taken. We show that the widely used lock-in technique performed while acquiring an STM topography in a closed feedback loop cannot be used to extract this local charge order from STS dI/dV differential conductance maps. In such situations, the use of the lock-in technique leads to systematically incorrect dI/dV measurements, giving a false local charge order. We show that a correct method is either to perform a constant height measurement or to perform a full grid of $dI/dV(V)$ spectroscopies, using a set point for the bias voltage outside the bandwidth of the correlated material where the local density of states (LDOS) is expected to be spatially homogeneous. We take as a paradigmatic example of two-dimensional material the 1/3 single-layer Pb/Si(111) phase. As large areas of this phase cannot be grown, charge ordering in this system is not accessible to angular resolved photoemission or grazing x-ray diffraction. Two previous investigations by STM/STS supplemented by *ab initio* density functional theory (DFT) calculations concluded that this material undergoes a phase transition to a low-temperature 3×3 reconstruction where one Pb atom moves up, the two remaining Pb atoms shifting down. A third STM/STS study by Adler *et al.* [F. Adler, S. Rachel, M. Laubach, J. Maklar, A. Fleszar, J. Schäfer, and R. Claessen, Phys. Rev. Lett. **123**, 086401 (2019)] came to the opposite conclusion, i.e., that two Pb atoms move up, while one Pb atom shifts down. We show that this latter erroneous conclusion comes from an artifact induced by the lock-in technique. In contrast, using a full grid of $dI/dV(V)$ spectroscopy measurements, our results show that the energy-dependent LDOS maps agree very well with state-of-the-art DFT calculations, confirming the one-up two-down charge ordering. We show that this structural and charge reordering inside the 3×3 unit cell is equally driven by electron-electron interactions and the coupling to the substrate.

I. INTRODUCTION

The understanding of the structural and electronic properties of correlated materials represents an important challenge in condensed matter physics. The interplay between Coulomb interactions and electrons delocalization leads to the appearance of new ground states often presenting charge, spin, and/or lattice reordering [1–10]. Probing experimentally these various orders with macroscopic and local probes is essential to provide solid grounds for advanced theoretical modeling. In addition, in the goal of reaching a quantitative understanding of the theoretical properties of correlated

electronic systems, it is highly desirable to find materials exhibiting the greatest chemical simplicity. The ideal situation is that of a small number of atoms in the unit cell possibly leading to a single narrow band crossing the Fermi level, isolated from other bulk bands and presenting strong on-site Coulomb repulsion. Such a system would ideally implement the single-band Hubbard model at the heart of the description of strongly correlated materials [11].

For a single-band Hubbard model in two dimensions (2D), depending on the precise lattice geometry and parameters of the hopping integrals, on-site Coulomb repulsion, as well as possible nonlocal repulsion terms, various phases are theoretically predicted as ground states. These range from paramagnetic metals with or without charge ordering to insulating states with various magnetic ordering or spin-liquid phases [12].

*m.calandrabuonaura@unitn.it
†christophe.brun@sorbonne-universite.fr

Such a paradigmatic situation seems at first glance to be realized in 2D in a class of surface crystals, called an α phase, consisting of a low-density single layer of tetravalent metal atoms (Pb or Sn) grown on tetravalent semiconducting substrates like Si(111) or Ge(111) [2,13–15]. The atoms are organized in a triangular lattice forming a $\sqrt{3} \times \sqrt{3}$-$R30°$ reconstruction in the high-temperature phase. Each metal atom leaves a free electron at T4 sites, leading to a single half-filled electronic band confined at the surface and isolated from bulk bands. The α-phase compounds offer a nice chemical simplification since there are only two different atoms in the unit cell having *s-p* hybridized orbitals. These materials are often considered as a prototypical realization of the single-band Hubbard model, despite the fact that this aspect has been recently questioned [16,17].

The theoretical consideration of the explicit coupling between the electronic, lattice, and substrate degrees of freedom seems mandatory for such surface-confined 2D materials, as already established for denser systems [18]. It is nevertheless at present taken into account only by *ab initio* density functional theory (DFT) methods [9,10,14,16,17,19] and is neglected in many-body ones (see, for instance, Refs. [20,21]). Which methods among advanced DFT methods, like DFT+U [22], HSE [23,24], or many-body ones are capable or not of describing the structural, electronic, and magnetic ordering taking place in these compounds should be looked at in detail by a precise comparison with all available experimental results for each particular material.

In a correlated surface material, both electron-phonon (*e*-ph) and electron-electron (*e-e*) effects can contribute to a lattice reordering. Experimentally, a 3×3 reconstruction is observed at low temperature for all α-phase compounds except Sn/Si(111). The lattice reconstruction can be inferred from surface x-ray diffraction (SXRD) only when the α-phase can be macroscopically and homogeneously grown, as done for Pb/Ge(111) and Sn/Ge(111) [25–27].

The situation is thus more challenging in Pb/Si(111), where a 3×3 reconstruction is observed at low temperature by scanning tunneling microscopy (STM) [5,16,28,29] but where the small size of the 3×3 domains coexisting with large $\sqrt{7} \times \sqrt{3}$ regions prevents SXRD or x-ray photoelectron spectroscopy (XPS) to be used to deduce the refined 3×3 structure [5,30]. In this case, the atomic lattice reconstruction and the associated electronic charge ordering has to be solely deduced from STM/scanning tunneling spectroscopy (STS) or atomic force microscopy (AFM) experiments, which necessitates an error-free protocol. With respect to this issue, the recent studies undertaken in Pb/Si(111) by STM/STS are illuminating as they present conflicting results and different interpretations [16,29].

In Ref. [16], Tresca *et al.* showed that at 300 mK the Pb/Si(111)-3×3 ground state is a correlated metal presenting a charge order. This correlated metallic state is characterized by a vertical lattice distortion, having one Pb atom up and two Pb atoms down (called one-up, two-down $1u2d$ in the following for simplicity). This structural deformation is accompanied by a local electronic ordering due to the fact that in the 3×3 unit cell, two electrons among three localize on the Pb up atom while the third unpaired electron is shared among the two-down Pb atoms ensuring metallicity.

Note that the same $1u2d$ atomic ordering was deduced earlier by Brihuega *et al.* from STM topography measurements confronted to DFT calculations in the generalized gradient approximation (GGA) approximation [5]. Additionally, SXRD measurements in Pb/Ge(111) and Sn/Ge(111) showed the same atomic ordering [26,27]. Surprisingly, the recent STM/STS study by Adler *et al.* of the local charge order in Pb/Si(111) came to the opposite conclusion, promoting a two-up, one-down ($2u1d$) atomic ordering [29].

In the present paper, we solve the controversy by demonstrating that it is related to an incorrect method to extract information on local order via the lock-in technique.

II. EXPERIMENTAL RESULTS

The α-Pb/Si(111) single-layer phase was prepared using a well-known procedure as described in Ref. [16]. This procedure results in the formation of a mixed phase consisting of dense, metallic, and large $\sqrt{7} \times \sqrt{3}$ domains having a Pb coverage of 1.2 ML adjoining small $\sqrt{3} \times \sqrt{3}$ regions of size less than 100 nm having a Pb coverage of 1/3 ML. Below about 86 K, the $\sqrt{3} \times \sqrt{3}$ regions transit to a 3×3 structure [5]. Our measurements were performed on 3×3 domains having a lateral size larger than 25 nm at $T = 0.3$ K, 2 K, or 4.2 K with metallic PtIr or W tips. For such range of domain sizes, we have found that the spectral characteristics presented hereafter are well established. The $I(V)$ spectra were measured far enough from boundaries with neighboring $\sqrt{7} \times \sqrt{3}$ domains to probe intrinsic electronic properties. The $dI/dV(V)$ spectra were obtained by numerical differentiation of the raw $I(V)$ curves. Negative (positive) bias voltage corresponds to occupied (empty) sample states.

Figure 1 shows a characteristic 3×3 domain measured by STM at $T = 4.2$ K. We used the same tunneling current ($I = 20$ pA) but two different bias voltages [$V_{bias} = -1.0$ V in Fig. 1(a) and $V_{bias} = +1.0$ V in Fig. 1(b)]. Strikingly, a contrast reversal exists between Figs. 1(a) and 1(b). In Fig. 1(a), the maxima of the $z(x, y)$ signal of the STM constant current topography features a triangular lattice of bright dots while in Fig. 1(b) it forms a honeycomb lattice. Moreover, the location of the bright dots in Fig. 1(a) corresponds to the location of the darker dots in Fig. 1(b). This can be seen better by inspecting Figs. 1(d) and 1(e), presenting a close-up of the region situated in the white square. The point defect present in this region features the absence of a bright dot in Fig. 1(d) and a darker dot in Fig. 1(e). It is presumably a Pb vacancy. Going away from this point defect enables a site-by-site comparison between Figs. 1(d) and 1(e).

Our detailed analysis of the experimental results, supplemented by the state-of-the-art *ab initio* DFT calculations presented below, allows us to conclude that the bright dots in Figs. 1(a) and 1(d) are associated to the Pb-up sites while the two bright dots forming the honeycomb lattice in Figs. 1(b) and 1(e) correspond to the atomic sites of the two Pb-down atoms. For clarity, green, and red dots are superposed on STM topographies Figs. 1(d) and 1(e) to represent the expected locations of the up and down atoms, respectively. Nevertheless, as we show now, this conclusion cannot solely be deduced from STM measurements. Indeed, the characteristic variation in height of the $z(x, y)$ signal measured in
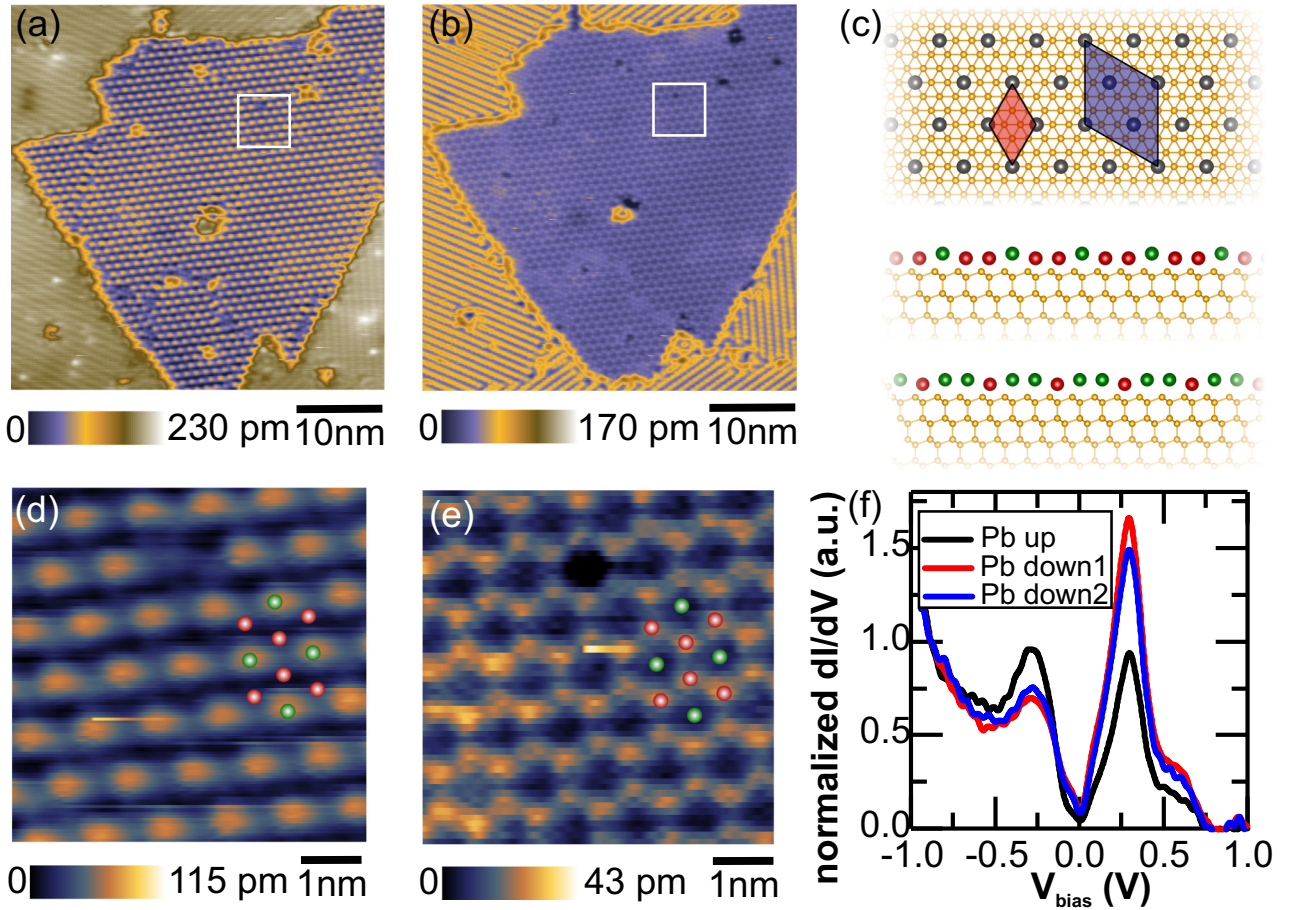
FIG. 1. All measurements presented in this figure were carried out at $T = 4.2$ K. (a) STM topography of a 3×3 domain measured with $V_{bias} = -1.0$ V and $I = 20$ pA. It shows the sample occupied states. (b) Same domain as in (a) but measured with $V_{bias} = +1.0$ V and $I = 20$ pA. It shows the sample unoccupied states. (c) Top: Top view of the high-temperature $\sqrt{3} \times \sqrt{3}$-R30° (red) and low-temperature 3×3 (blue) unit cells of α-Pb/Si(111). Bottom: Side view of the 3×3 $1u2d$ and $2u1d$ phases. (d) Close-up of the area delimited by the white rectangle in (a). It features a triangular lattice of dots associated to the Pb-up atoms. The colored balls indicate the theoretical location of the Pb atoms associated with the $1u2d$ phase. (e) same as in (d) but for $V_{bias} = +1.0$ V and $I = 20$ pA. A characteristic honeycomb lattice is seen associated with the two-down atoms. (f) dI/dV spectra measured by STS proportional to the LDOS of the three different Pb atoms present in the 3×3 unit cell denoted Pb-up (black curve), Pb-down1 (red curve), and Pb-down2 (blue curve). Set point for STS $V_{bias} = -1.0$ V and $I = 100$ pA.

Fig. 1(d) [respectively, Fig. 1(e)] is very small: it is only of about 0.20 Å. This small value suggests that there could be, in principle, two effects contributing to it. There could be (i) a difference in the vertical height (i.e., in the direction perpendicular to the surface) of the three Pb atoms inside the 3×3 unit cell and/or (ii) a difference in their integrated local density of states (LDOS) for the occupied (respectively, unoccupied) states. As we show hereafter, only a detailed comparison with advanced *ab initio* DFT calculations enables us to conclude which effects take place and whether there is or not an atomic reconstruction. Nevertheless, since we aim at concluding whether or not there is an atomic reconstruction accompanied by possible charge ordering on the various Pb sites, we need to perform site-dependent STS measurements to probe the corresponding spatial variations of the LDOS at the atomic scale.

Site-dependent STS measurements are presented in Fig. 1(f). The characteristic dI/dV spectra of the three different Pb sites seen by STM inside the 3×3 unit cell

are shown. These spectra are consistent with the spatially averaged dI/dV spectrum presented in our previous work (see Fig. 1(c) in Ref. [16]). In particular, all three spectra reveal a strongly depressed DOS at ε_F not reaching zero, which is a hallmark of the correlated semimetallic character of the surface. This depressed DOS at ε_F is surrounded by two prominent peaks located almost symmetrically with respect to ε_F at -0.3 eV and $+0.3$ eV. At larger binding energy, i.e., between $-1.0 < V < -0.5$ eV, the conductance strongly increases due to the LDOS associated to Si bands [16]. In the unoccupied states, a sharp drop in conductance occurs above the main peak and negative differential conductance is measured between $\simeq 750$ meV and 1 V.

A. Probing charge ordering at the atomic scale through LDOS maps with scanning tunneling spectroscopy: Methodological considerations

Since we need and want to compare with one another the LDOS measured on each of the three different Pb sites seen

in the 3×3 unit cell by STM, we need to be sure that the site-dependent dI/dV spectra are measured in a way that enables such a spatial comparison. Ideally, according to the Tersoff-Hamann theory of STM, the LDOS should be probed at constant tip-sample height to enable such a correct spatial comparison [31]. If this condition is fulfilled, then each $dI/dV(V)$ spectrum measured over the surface is proportional to the sample LDOS and a direct spatial comparison is possible. Let us note that the contribution of the tip DOS to the $dI/dV(V)$ signal is neglected in the Tersoff-Hamman approximation: the tip DOS is assumed to be constant around ε_F. Furthermore, it is also assumed that the spectroscopic measurements are performed in a small enough energy range around ε_F such that the transmission coefficient does not vary appreciably in this energy range. This is typically verified for an energy interval of $[-1;+1]$ eV around the Fermi level and a tip work function larger than 4 eV.

In practice, performing constant-height $I(V)$ spectroscopies with STM is challenging. The reason is that this condition requires us to precisely determine a plane parallel to the sample surface along which the tip can be scanned with an open feedback loop. Due to the small thermal drift existing along the $z(x, y)$ direction, it is usually not possible with this method to perform more than several hundreds of $I(V, x, y)$ spectra. Thus full 2D $I(V, x, y)$ spectroscopy grids with high spatial resolution over areas larger than a few nm^2 are usually impossible. It is nevertheless possible to perform STS measurements under constant tip height using a lock-in technique for a given voltage V. This is much less time-consuming and has been demonstrated for a variety of systems. This issue was first discussed in the context of surface states of noble metals [32,33]. The LDOS above adatoms [33], single molecules [34], or supramolecular networks [35] over small areas could also be measured this way. An additional method going beyond constant-height measurements has also been proposed to deal with the case of nano objects adsorbed on surfaces and improve the deficiency of the constant-height method in this case [36].

The principle of lock-in in the detection technique is to directly acquire the $dI/dV(V, x, y)$ signal by adding a small ac voltage $V_{ac}\cos(\omega t)$ to the DC bias voltage V applied between tip and sample. The $dI/dV(V, x, y)$ signal is obtained from a demodulation by the lock-in amplifier according to the first-order approximate relation:

$I(V + V_{ac}, x, y) = I(V, x, y) + dI/dV(V, x, y)V_{ac}\cos(\omega t)$. This technique can be used in constant height mode with an open feedback loop, as mentioned above. In this case, it leads to correct LDOS measurements since it fulfils the Tersoff-Hamman condition. Nevertheless, stringent time limitations exist for the STS measurements in a dense grid mode due to the open feedback loop, as explained above. In contrast, if the lock-in technique is used in a closed feedback loop while scanning the STM tip in constant current mode, it fails to reveal the true LDOS for energy-dependent and/or site-dependent LDOS, as is usually the case for materials presenting (strong) electronic correlations together with charge ordering. An example of this failure is provided by the data of Adler *et al.* presented in Ref. [29] and reproduced in the present Fig. 2 for our correlated 2D Pb/Si(111) material. The reason for this failure is that the constant current condition

dramatically changes and can even reverse the relative LDOS weight of atomic sites presenting different LDOS energy dependencies and/or charge ordering.

If one aims at performing a dense 2D and full $I(V, x, y)$ spectroscopy grid, as we need here, that typically contains from several thousands to several tens of thousands of individual $I(V, x, y)$ spectra (taking from about ten to several tens of hours of measurement), the usual trick is to work under closed feedback loop conditions by choosing an appropriate common set point (I_0, V_0) for each $I(V, x, y)$ spectroscopy. This last method has been widely used in STS experiments for about 20 years, including, for instance, complex materials where electronic correlations play an important role such as high-temperature cuprate superconductors [37]. In this case, the $dI/dV(V, x, y)$ spectra are obtained by numerical differentiation of the $I(V, x, y)$ curves. It can directly be seen that for this latter method to be correct, the choice of the (I_0, V_0) set point should qualitatively reflect the constant-height condition. Thus, in each particular situation and material, depending on the energy range that is to be measured, care should be taken regarding the choice of the (I_0, V_0) set point. Fortunately, for many materials there often exists an energy range $[eV_1, eV_2]$ for which the LDOS is homogeneous over the area of interest, which enables a postnormalization procedure of the $dI/dV(V, x, y)$ spectra. This corresponds to the procedure that we have followed and that will be further explained below.

B. Probing charge ordering at the atomic scale through LDOS maps with scanning tunneling spectroscopy: The case of 1/3 monolayer Pb/Si(111)

From Fig. 1, we see that the actual measured bandwidth of the 3×3-Pb/Si(111) phase is about $[-0.5;+0.5]$ eV. To extract a meaningful local $dI/dV(E, x, y)$ signal proportional the intraunit cell LDOS, we have chosen to measure a 200×200 grid of single $I(V, x, y)$ curves between $[-1;+1]$ eV with a common set point for each STS spectroscopy at $I_0 = 100$ pA, $V_0 = -1.0$ V. This dense set of $dI/dV(E, x, y)$ data is obtained from numerical differentiation of the corresponding single $I(V, x, y)$ curves. The set point in voltage is chosen far in energy from the 2D surface band of interest. In particular, as our DFT calculations presented below show, this set point is chosen well enough in the silicon bulk valence band so no peculiar site dependence exists in the LDOS for $E \approx eV_0$. This means that it is possible to postnormalize the measured $dI/dV(V, x, y)$ spectra at the energy $E \approx eV_0$. This is exactly the procedure that we have followed here. One can also note that the same normalization procedure was performed in Fig. 1(f). As a consequence, our reference $dI/dV(E = -1eV, x, y)$ map shown in the first row of Fig. 2(a) presents a homogeneous aspect. This spectroscopic behavior is well reproduced by our optimized DFT calculations presented in the first row of Fig. 2(b), evaluating the LDOS for the $1u2d$ phase at a height of 3 Å from the topmost Pb atoms.

The panels in Fig. 2(a) present $dI/dV(E, x, y)$ maps obtained following this protocol for various energies E running through the whole 2D correlated surface bands. Let us note that the conductance color scale of each $dI/dV(E, x, y)$ map is identical (having conductance values between 0 and 2.5). This enables a proper quantitative comparison of the LDOS
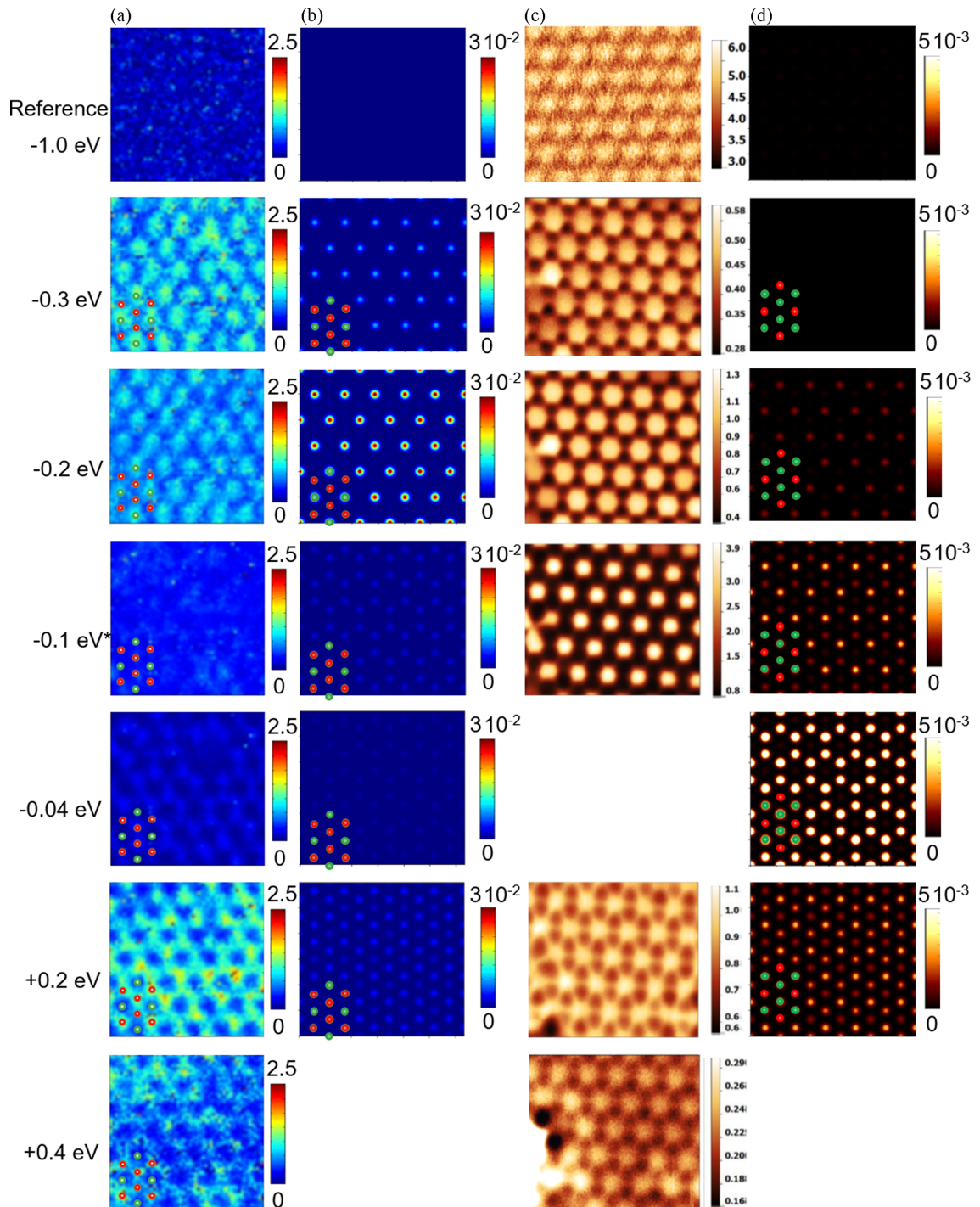
FIG. 2. Comparison of the energy-resolved LDOS maps of the 3×3-Pb/Si(111) phase measured at 4 K by STS using two different methods, confronted to DFT calculations for the optimized $1u2d$ (column b) and $2u1d$ (column d) phases. Column a) represents this work. It shows $dI/dV(E, x, y)$ maps numerically derivated from a grid of 200×200 $I(V, x, y)$ curves acquired between [-1;+1] eV with a common set-point for each spectroscopy at $I_0 = 100$ pA, $V_0 = -1.0$ V. Each row has a different bias adopted for the measurement, the corresponding energy E being indicated in eV. The normalized conductance color scale is identical for all these panels and is shown by a vertical bar (having $dI/dV(E, x, y)$ values between 0 and 2.5) on the right of each map. Column b) is the theoretical LDOS for the $1u2d$ phase while in column d) the theoretical LDOS for the proposed $2u1d$ system is reported. The theoretical panels are presented with a common color scale for each phase, namely between 0 and 3 10^{-2} states/Ry for the $1u2d$ (respectively, 0 and 5 10^{-3} states/Ry for the $2u1d$). The colored balls in columns a) and b) feature the theoretical location of the Pb atoms associated to the one up-two down phase. In column c) we reproduce the $dI/dV(E, x, y)$ maps by Adler *et al.* [29], for comparison. The measurements of by Adler *et al.* are obtained by using a lock-in technique and acquired in closed feedback loop together with the STM topography at the corresponding voltage. In these measurements the conductance color scale vary for each energy E, which we indicated accordingly. Note also that we have rotated by 90° these LDOS images in order to enable a direct comparison with ours. For the energy $E = -0.1$ eV*, the map in column a) was in fact obtained at an exact energy of -0.115 eV.

measured at different energies. The three different Pb atoms are superposed with lighter (green) color for the up atoms and darker (red) color for the down ones. These experimental $dI/dV(E, x, y)$ maps can be directly compared to the panels in Fig. 2(b) showing our optimized DFT calculations of the LDOS for the $1u2d$ phase evaluated at a height of 3 Å from the topmost Pb atoms.

At larger binding energy $E \approx -0.3$ eV, close to the peak observed in the LDOS of the occupied states, our measurements show that the LDOS is maximum on the up atoms, in agreement with Fig. 1(f). For this energy, the dominant LDOS signal forms a triangular lattice of bright dots associated to the Pb-up atoms. This LDOS behavior is precisely reproduced by DFT calculations of the $1u2d$ phase, even if theoretically, the LDOS maximum on the Pb up atoms is obtained for slightly smaller energy $E \approx -0.2$ eV. When the binding energy E reduces for $-0.3 \leqslant E \leqslant -0.115$ eV, the experimental LDOS on all sites reduces. Simultaneously, the relative LDOS weight between the up and down atoms also reduces. When one reaches $E \approx -0.115$ eV, the LDOS becomes approximately equal on all three Pb sites, as seen by the homogeneous color, in agreement with Fig. 1(f). Theoretically, such behavior is also predicted to occur around $E = -0.1$ eV, as shown by our theoretical predictions.

For $E \geqslant -0.115$ eV, the relative LDOS weight reverses, the LDOS becoming larger on the down atoms than on the up ones, as expected from Fig. 1(f). This behavior is well reproduced by DFT calculations. Between $0 \leqslant E \leqslant 0.3$ eV, the LDOS rises on all three Pb sites and the relative weight between the down and up sites also increases. This is illustrated for $E \approx +0.2$ eV, where one sees that the LDOS weight on the two down atoms is almost equal and dominates. As a result, the dominant LDOS signal forms a honeycomb lattice. This honeycomb lattice presents a complete site-reversed contrast with respect to the triangular lattice seen for $E = -0.3$ eV. The theoretical results agree with this picture. When reaching energies close to the upper band edge, both the LDOS and relative weight between the up and down sites diminish. Furthermore, slight inhomogeneities between sites of the same type become visible, probably induced by disorder effects. The theoretical bandwidth being slightly smaller than the measured one, the comparison cannot be made for this latter energy.

C. Probing charge ordering at the atomic scale through LDOS maps with scanning tunneling spectroscopy: On artifacts induced by the lock-in technique

Our atomically resolved LDOS measurements inside the Pb-3×3 unit cell are in strong contrast with the previously reported STS results by Adler *et al.* [29]. A detailed comparison is provided for similar energies in Fig. 2. For large binding energies ($E \approx -0.3$ eV), the LDOS map is similar to ours, revealing a triangular lattice of bright dots. However, as the energy increases, the LDOS contrast never qualitatively changes in Adler *et al.*'s data. For instance, the LDOS weight reduction around ε_F is not observed, nor the LDOS reversal between the up and down atoms for $E \geqslant -0.115$ eV. Instead, Adler *et al.*'s measurements suggest that the LDOS is always dominated by the same type of atoms for all energies inside

the bandwidth. This is physically implausible. This is also opposite to our experimental measurements and theoretical analysis, the latter being detailed below in Sec. III, since in our modeling we also considered the possibility of the formation of the $2u1d$ phase.

Furthermore, the $dI/dV(E, x, y)$ maps presented by Adler *et al.* are themselves in contradiction with their own site-dependent $dI/dV(V, x, y)$ spectra presented in Fig. S4 of the Supplemental Material of Ref. [29]. Indeed, from Fig. S4, the site-dependent $dI/dV(V, x, y)$ spectra show a qualitative behavior similar to the one presented in Fig. 1(f). This shows that for $E \lesssim -0.1$ eV their $dI/dV(E, x, y)$ maps should be dominated by the LDOS measured on what they called "center" atoms (Pb up atoms in our case). Then an almost equal LDOS weight should be observed around ≈ -0.1 eV between the denoted center and corner atoms (Pb-down atoms in our case), followed by an LDOS contrast reversal for $\approx -0.1 \leqslant E \leqslant \approx +0.3$ eV. This expected energy dependence is clearly not what is measured in the $dI/dV(E, x, y)$ maps of Ref. [29], which we reproduced in Fig. 2. This experimental artifact, leading to erroneous LDOS measurements, is due to the improper use of the lock-in technique in a closed feedback loop while acquiring the STM topography for a correlated 2D material presenting site-dependent LDOS and charge ordering, as we explained before in Sec. II A.

Another unfortunate consequence of the artifacts induced by the lock-in technique to acquire $dI/dV(V, x, y)$ maps in closed feedback loop deals with quasiparticle interference (QPI) measurements. QPI measurements are a phase-coherent manifestation of the scattering of elementary electron or hole excitations by defects [38]. These QPI measurements are typically obtained by performing the Fourier transform of a $dI/dV(V, x, y)$ map measured for a given energy. Since we just saw that $dI/dV(V, x, y)$ maps acquired in a closed feedback loop are incorrect for site-dependent LDOS, one deduces that QPI maps will also be incorrect. This is particularly important to note since this technique is broadly used to infer information about order parameter symmetry, topology, spin, and band-structure properties [39,40]. We thus may consider with care the recent QPI experiments done this way in α-phase materials [29,41]. Evidence for this situation is provided by comparing the QPI maps at the Fermi level for Pb-3×3/Si(111) obtained using our method (see Fig. 3 in Ref. [16]) and Adler's (see Fig. 3 in Ref. [29]).

To support the presented experimental STM/STS results and their interpretation, we now present and discuss in detail the theoretical investigations of the 1/3 ML α-Pb/Si(111) phase using advanced DFT calculations.

III. THEORY: MODELING THE STRUCTURAL AND ELECTRONIC PROPERTIES OF THE CORRELATED 1/3 MONOLAYER PB/SI(111)

A. Computational details

As in Ref. [17], we model the Pb/Si(111) surfaces by considering a layer of Pb atoms on top of three or six Si bilayers. The bottom dangling bonds are capped with hydrogen atoms fixed to the relaxed positions obtained by capping one side of the pristine Si surface. The atomic position of the

first five (four) Si-substrate layers below the Pb single layer are optimized whereas the remaining seven (two) layers are fixed to the Si bulk positions. More than 15 Å of vacuum is included.

DFT calculations are performed with QUANTUM ESPRESSO [42,43] and CRYSTAL17 [44,45] codes. For plane-wave calculations, we used ultrasoft pseudopotentials with the same settings of Ref. [16]. We used the following semilocal approximations for the exchange and correlation kernel: the local density approximation (LDA), the GGA, and the GGA+U approximation with an energy cutoff up to 45 Ry. Integration over the Brillouin zone (BZ) was performed using uniform $10(6) \times 10(6) \times 1$ Monkhorst and Pack grids [46] for the $\sqrt{3} \times \sqrt{3}$-R30^o(3×3) and a 0.001 Ry Gaussian smearing.

Hybrid-functional calculations in plane waves for cells as large as those considered here are hardly feasible. Thus, HSE06 [23,24] (nonrelativistic) calculations were performed by using the CRYSTAL17 [44,45] code with Gaussian basis sets exactly as in Ref. [17]. The basis sets used for these calculations have been directly downloaded from the CRYSTAL web site. For Pb, we used pseudopotentials [47,48] from the CRYSTAL distribution, while for Si and the capping H an all-electron m-6-311G(d) [49,50] and TZVP [51] have been, respectively, adopted.

Integration over the BZ was performed with the same k-mesh density as in the plane wave calculation and a Fermi-Dirac smearing of 0.0005 Ha. The integration threshold was set to 10^{-7} for integrals in the Coulomb series and 10^{-7}, 10^{-15}, and 10^{-30} for the exchange ones (see Refs. [44,45] for more details).

In this framework, we optimize the internal coordinates.

Relativistic effects are not implemented in the CRYSTAL17 code. To overcome this difficulty, in analogy with Ref. [17], we fit the nonrelativistic HSE06 electronic structure and Fermi surfaces at HSE06 fixed geometry in a DFT+U formalism with U on the Pb and Si p states, and then apply noncollinear spin orbit on top at fixed atomic coordinates in a DFT+U+SOC calculation. This is possible because relativistic effects are negligible in the atomic relaxation process [16,17], vice versa a good description of the energy gap of Si is necessary for the structural prediction.

B. Determination of the ground state

As known, at low temperature the α-Pb/Si(111) shows a charge density wave (CDW) transition between the $\sqrt{3} \times \sqrt{3}$-R30^o periodicity to the 3×3 ordering with three inequivalent Pb atoms [2,5,16,25,29,30,52–55]. For years, the 3×3 phase in Pb/Si(111) has been interpreted as a deformation in which one Pb atom is higher and the other two closer to the substrate, in analogy with the similar Pb/Ge(111) [2,17,25,52,54]. This reconstruction is usually labeled one up and two down (1u2d). Our previous works [16,17] showed that the electron-electron interaction is important in this system and, in particular, the nonlocal exchange interaction among the Pb electrons and the Si substrate [17]. Furthermore, we have shown that the spin-orbit interaction plays an important role. As mentioned, this aspect has been recently questioned by an experimental/theoretical work claiming that

the low-temperature Pb/Si(111) ground state would appear to be the two-up and one-down structure (2u1d) [29].

To reconcile this disagreement, as a first step, we studied the stability of both 1u2d and 2u1d CDWs with different functionals and different substrate thickness modelization. Results are summarized in Table I.

At the semilocal functional level (LDA and GGA), for the 1u2d CDW phase, we obtain the results already known in literature [16,55,56] and we find that the 2u1d phase is not stable.

We repeated the calculation by including a moderate and strong Hubbard term on Pb sites (2 and 8 eV, respectively). The specific values adopted for U are not physically representative—just serve as a computational knob to study the correlation effects in high and low regimes. As summarized in Table I, the only case able to describe the 2u1d CDW phase as a ground state is the inclusion of a correlation term of 8 eV on Pb atoms. As mentioned, the eventual physical justification for such a high value is far from trivial and makes this hypothesis a mere stylistic exercise. Furthermore, in such a case the height difference found between up and down Pb atoms is ~1.9 Å, a completely unrealistic value.

On the contrary, predictions with hybrid functionals (HSE06) have proven to be extremely accurate for the similar compound α-Pb/Ge(111) [17] due to the strong hybridization of the Pb valence electronic wave functions with the ones of the substrate atoms, as also noticed previously for Sn/Ge(111) and Sn/Si(111) [57,58]. In the α-Pb/Si(111) case, the HSE06 calculations predict the 1u2d CDW to be the ground state. The 2u1d phase is never stable. Even starting from the 2u1d, during the relaxation process, the system escapes from this configuration to adopt the 1u2d deformation.

However, even assuming a doubtful failure of the well-known predictive power of the DFT, we tried to calculate the electronic properties of the hypothetical 2u1d system, using a structure as close as possible to that experimentally declared in Ref. [29]. Therefore, we model the system considering the substrate in its ideal positions and three Pb adatoms in the T4 site: one at 1.90 Å and two at 2.57 Å from the Si substrate, thus using the distortion (Δh) reported in Ref. [29] for the 2u1d phase.

Comparing our theoretical DOS prediction for the 2u1d proposed system (see Fig. 3, top) with the experimental Pb-resolved STS spectra [see Fig. 1(f)], one sees that a double up contribution higher in the filled state region and lower in the empty state region should be observed in contrast with the experimental data showing an exact opposite behavior. This qualitative difference is also reflected in the experimental LDOS behavior presented in Fig. 2. This set of arguments strongly supports our interpretation and modeling in terms of the 1u2d structure.

Another important aspect discussed already in Sec. II B is the presence of a balanced point: by this term, we mean the energy for which the partial DOS contributions from the different Pb atoms are approximately equal in the unit cell. Therefore, at this energy, the LDOS map should appear (almost) flat and homogeneous. We identify this balanced point to be ~ + 0.07 eV in the ideal 2u1d structure and ~ − 0.13 eV for the HSE06-relaxed 1u2d one. The balanced point is predicted to be positive in 2u1d and negative in the

TABLE I. Stability of the different phases of 1/3 monolayer Pb/Si(111) simulated with three and six Si bilayers. The high-temperature phase is labeled $\sqrt{3} \times \sqrt{3}$. The energy differences are referred with respect to the ground state (in bold). All energies are expressed in eV/Pb. The acronym NS means not stable.

	Three bilayers			Six bilayers		
	$\sqrt{3} \times \sqrt{3}$	3×3 (1*u*2d)	3×3 (2*u*1d)	$\sqrt{3} \times \sqrt{3}$	3×3 (1*u*2d)	3×3 (2*u*1d)
LDA	**0.000**	+0.000	+0.000	**0.000**	+0.000	+0.001
GGA	+0.005	**0.000**	+0.004	+0.001	**0.000**	+0.001
GGA+U ($U = 2$ eV)	+0.008	**0.000**	+0.007	+0.003	**0.000**	+0.003
GGA+U ($U = 8$ eV)	+0.296	+0.141	**0.000**	+0.155	+0.137	**0.000**
HSE06	+0.026	**0.000**	*NS*	+0.023	**0.000**	*NS*

1*u*2d case. This negative value of ~ -0.13 eV for the balanced point of the 1*u*2d phase is in excellent agreement with our experimental results where it occurs around ~ -0.115 eV [compare first the spectra in Fig. 1(f) with the ones in Fig. 3, bottom, and then look at the homogeneous conductance map seen in Fig. 2(a) for $E = -0.1$ eV].

To enable a direct comparison between theoretical atom-projected DOS and experimental LDOS maps, we evaluated the *ab initio* theoretical LDOS at a height of 3 Å from the topmost Pb atom(s). The results are summarized in Fig. 2(b) for the 1*u*2d phase and Fig. 2(d) for the 2*u*1d one.

FIG. 3. Predicted Pb atom-projected DOS for the ideal 2*u*1d CDW (top) and for the 1*u*2d one (bottom). In the top panel, the high peak at ~ -0.42 eV is an artificial structure due to the impossibility of relaxing the system. Blue curves features the Pb^{up} contributions, orange the Pb^{down} ones. Please note that the balanced point, defined as the energy around which the projected DOS of the up atom(s) cross the one of the down atom(s), is located at opposite energies for the 2*u*1d and 1*u*2d CDW (positive and negative, respectively). Also, these results were obtained at the GGA+U+SOC level (as described in Sec. III).

These results confirm once more the correctness of our measurement method and the fact that low-temperature α-Pb/Si(111) adopts the 1*u*2d CDW phase. In fact, the 1*u*2d theoretical results are in good agreement with experiments, apart from the absolute values of the bias at which we make the comparisons. This last aspect is due to a nonperfect description of the electronic renormalization, but the general trend is properly described: for low energies, (see Fig. 2) we observe a triangular lattice linked to the filled Pb-up states. Near the balanced point, the intensity of the LDOS map is small and rather homogeneous. For larger energies, the transition to the honeycomb pattern, linked to the Pb-down states, is evident.

For what concerns the ideal 2*u*1d configuration, the triangular lattice is evident around -0.2 eV. However, the honeycomb pattern, related to the two Pb-up atoms, appears immediately for higher energies and remains extremely evident up to energies very close to the Fermi level. Furthermore, a contrast reversal in the LDOS map should also occur in this case due to the existence of a balanced point.

Finally, thanks to our ground-state DFT predictions (see Table I) and to the spectroscopic results in good agreement with the DFT ones, we can definitively conclude that the correlated α-Pb/Si(111) low-temperature CDW phase is the one-up, two-down reconstruction.

IV. CONCLUSION

In this paper, we addressed general issues and showed correct ways to extract the local charge order in 2D systems from STM/STS measurements. We showed that particularly important care should be taken when the charge order presents spatial variations at the atomic scale inside the unit cell. In such situations, we showed that the widely used lock-in technique, performed while acquiring an STM topography in a closed feedback loop, fails to extract this local charge order from STS dI/dV differential conductance maps. In contrast, a correct method is either to perform a constant height measurement or to perform a full grid of $dI/dV(V)$ spectroscopies, using a set point for the bias voltage outside the bandwidth of the 2D material where the LDOS is expected to be spatially homogeneous.

We have demonstrated our ideas using as a paradigmatic example of 2D material the 1/3 single-layer $\sqrt{3} \times \sqrt{3}$-R30°-Pb/Si(111) phase, which presents strong electron-electron interaction. As large areas of this phase cannot be grown, the charge ordering in this system is not accessible to macroscopic
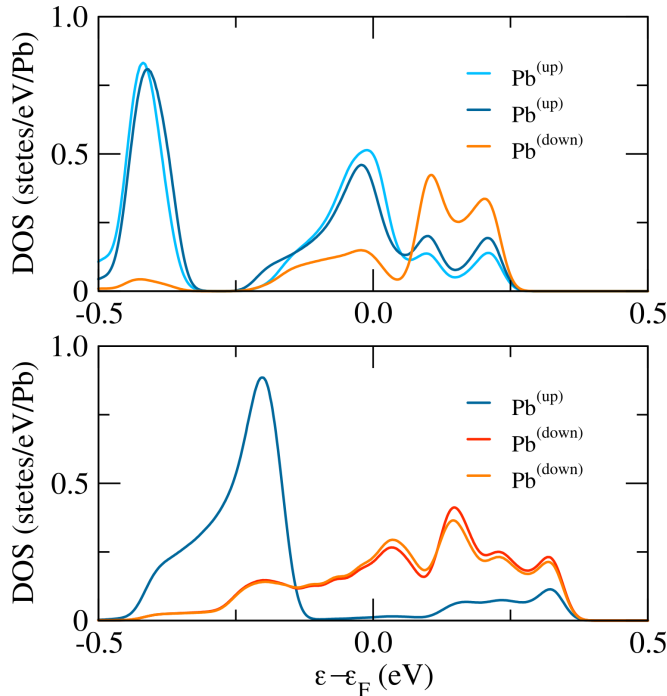
probes like ARPES or grazing x-ray diffraction, but can be determined only by local probes.

Our combined experimental and theoretical study enabled us to establish definitely that the low-temperature charge ordering in $\sqrt{3} \times \sqrt{3}$-$R30°$-Pb/Si(111) is associated with the one-Pb-up two-Pb-down 3×3 atomic reconstruction. The detailed comparison between STS energy-dependent LDOS maps and state-of-the-art DFT calculations agrees very well. Additionally, we show that this structural and charge reordering inside the 3×3 unit cell is equally driven by electron-electron interaction and the coupling to the surface. An important output of our results is that theoretical many-body approaches, neglecting the coupling to the substrate degrees of freedom, miss a proper description of these 2D correlated systems located at the surface plane of bulk crystals.

The described procedure and our considerations are fully general. They should be applicable to any material presenting a local atom-dependent charge ordering measured using the STM/STS technique, i.e., oxides like manganites [59] or iridates [60], quasi-1D or quasi-2D organic conductors [61,62], Mott insulators [8], ultrathin films or monolayers of transition metal dichalcogenides [9,10], twisted graphene bilayers [63], and so on.

[1] P. Fazekas and E. Tosatti, Physica B+C **99**, 183 (1980).

[2] J. M. Carpinelli, H. H. Weitering, E. W. Plummer, and R. Stumpf, Nature (London) **381**, 398 (1996).

[3] J. M. Carpinelli, H. H. Weitering, M. Bartkowiak, R. Stumpf, and E. W. Plummer, Phys. Rev. Lett. **79**, 2859 (1997).

[4] L. Ottaviano, M. Crivellari, L. Lozzi, and S. Santucci, Surf. Sci. **445**, L41 (2000).

[5] I. Brihuega, O. Custance, R. Pérez, and J. M. Gómez-Rodríguez, Phys. Rev. Lett. **94**, 046101 (2005).

[6] G. Ghiringhelli, M. L. Tacon, M. Minola, S. Blanco-Canosa, C. Mazzoli, N. B. Brookes, G. M. D. Luca, A. Frano, D. G. Hawthorn, F. He et al., Science **337**, 821 (2012).

[7] R. Comin, A. Frano, M. M. Yee, Y. Yoshida, H. Eisaki, E. Schierle, E. Weschke, R. Sutarto, F. He, A. Soumyanarayanan et al., Science **343**, 390 (2014).

[8] E. Janod, J. Tranchant, B. Corraze, M. Querré, P. Stoliar, M. Rozenberg, T. Cren, D. Roditchev, V. Ta Phuoc, M.-P. Besland et al., Adv. Funct. Mater. **25**, 6287 (2015).

[9] M. Calandra, Phys. Rev. Lett. **121**, 026401 (2018).

[10] C. Tresca and M. Calandra, 2D Mater. **6**, 035041 (2019).

[11] J. Hubbard, Proc. R. Soc. A **276**, 238 (1963).

[12] L. Balents, Nature (London) **464**, 199 (2010).

[13] G. Santoro, S. Scandolo, and E. Tosatti, Phys. Rev. B **59**, 1891 (1999).

[14] G. Profeta and E. Tosatti, Phys. Rev. Lett. **98**, 086401 (2007).

[15] P. Hansmann, T. Ayral, L. Vaugier, P. Werner, and S. Biermann, J. Phys.: Cond. Matter **25**, 094005 (2013).

[16] C. Tresca, C. Brun, T. Bilgeri, G. Menard, V. Cherkez, R. Federicci, D. Longo, F. Debontridder, M. D'angelo, D. Roditchev et al., Phys. Rev. Lett. **120**, 196402 (2018).

[17] C. Tresca and M. Calandra, Phys. Rev. B **104**, 045126 (2021).

[18] C. Brun, T. Cren, and D. Roditchev, Supercond. Sci. Technol. **30**, 013003 (2017).

[19] G. Profeta, A. Continenza, L. Ottaviano, W. Mannstadt, and A. J. Freeman, Phys. Rev. B **62**, 1556 (2000).

[20] G. Li, M. Laubach, A. Fleszar, and W. Hanke, Phys. Rev. B **83**, 041104(R) (2011).

[21] P. Hansmann, T. Ayral, L. Vaugier, P. Werner, and S. Biermann, Phys. Rev. Lett. **110**, 166401 (2013).

[22] M. Cococcioni and S. de Gironcoli, Phys. Rev. B **71**, 035105 (2005).

[23] J. Heyd, G. E. Scuseria, and M. Ernzerhof, J. Chem. Phys. **118**, 8207 (2003).

[24] J. Heyd, G. E. Scuseria, and M. Ernzerhof, J. Chem. Phys. **124**, 219906 (2006).

[25] A. Mascaraque, J. Avila, J. Alvarez, M. C. Asensio, S. Ferrer, and E. G. Michel, Phys. Rev. Lett. **82**, 2524 (1999).

[26] J. Zhang, Ismail, P. J. Rous, A. P. Baddorf, and E. W. Plummer, Phys. Rev. B **60**, 2860 (1999).

[27] O. Bunk, J. H. Zeysing, G. Falkenberg, R. L. Johnson, M. Nielsen, M. M. Nielsen, and R. Feidenhans'l, Phys. Rev. Lett. **83**, 2226 (1999).

[28] O. Custance, J. Gómez-Rodríguez, A. Baro, L. Juré, P. Mallet, and J.-Y. Veuillen, Surf. Sci. **482**, 1399 (2001).

[29] F. Adler, S. Rachel, M. Laubach, J. Maklar, A. Fleszar, J. Schäfer, and R. Claessen, Phys. Rev. Lett. **123**, 086401 (2019).

[30] I. Brihuega, O. Custance, M. M. Ugeda, and J. M. Gómez-Rodríguez, Phys. Rev. B **75**, 155411 (2007).

[31] J. Tersoff and D. R. Hamann, Phys. Rev. B **31**, 805 (1985).

[32] J. Li, W.-D. Schneider, and R. Berndt, Phys. Rev. B **56**, 7656 (1997).

[33] M. Ziegler, N. Néel, A. Sperl, J. Kröger, and R. Berndt, Phys. Rev. B **80**, 125402 (2009).

[34] X. Lu, M. Grobis, K. H. Khoo, S. G. Louie, and M. F. Crommie, Phys. Rev. Lett. **90**, 096802 (2003).

[35] W. Krenner, D. Kuhne, F. Klappenberger, and J. Barth, Sci. Rep. **3**, 1454 (2013).

[36] G. Reecht, B. Heinrich, H. Bulou, F. Scheurer, L. Limot, and G. Schull, New J. Phys. **19**, 113033 (2017).

[37] O. Fischer, M. Kugler, I. Maggio-Aprile, C. Berthod, and C. Renner, Rev. Mod. Phys. **79**, 353 (2007).

[38] L. Simon, C. Bena, F. Vonau, M. Cranney, and D. Aubel, J. Phys. D **44**, 464010 (2011).

[39] L. Chen, P. Cheng, and K. Wu, J. Phys.: Condens. Matter **29**, 103001 (2017).

[40] C.-L. Lin, N. Kawakami, R. Arafune, E. Minamitani, and N. Takagi, J. Phys.: Condens. Matter **32**, 243001 (2020).

[41] F. Ming, S. Johnston, D. Mulugeta, T. S. Smith, P. Vilmercati, G. Lee, T. A. Maier, P. C. Snijders, and H. H. Weitering, Phys. Rev. Lett. **119**, 266802 (2017).

[42] P. Giannozzi, S. Baroni, N. Bonini, M. Calandra, R. Car, C. Cavazzoni, D. Ceresoli, G. Chiarotti, M. Cococcioni, I. Daboand *et al.*, J. Phys.: Condens. Matter **21**, 395502 (2009).

[43] P. Giannozzi, O. Andreussi, T. Brumme, O. Bunau, M. B. Nardelli, M. Calandra, R. Car, C. Cavazzoni, D. Ceresoli, M. Cococcioni *et al.*, J. Phys.: Condens. Matter **29**, 465901 (2017).

[44] R. Dovesi, A. Erba, R. Orlando, C. M. Zicovich-Wilson, B. Civalleri, L. Maschio, M. Rérat, S. Casassa, J. Baima, S. Salustro *et al.*, Wiley Interdiscip. Rev.: Comput. Mol. Sci. **8**, e1360 (2018).

[45] R. Dovesi, V. R. Saunders, C. Roetti, R. Orlando, C. M. Zicovich-Wilson, F. Pascale, B. Civalleri, K. Doll, N. M. Harrison, I. J. Bush *et al.*, CRYSTAL17 User's Manual (2018), https://www.crystal.unito.it/Manuals/crystal17.pdf.

[46] H. J. Monkhorst and J. D. Pack, Phys. Rev. B **13**, 5188 (1976).

[47] G. Sophia, P. Baranek, C. Sarrazin, M. Rérat, and R. Dovesi, Phase Transit. **86**, 1069 (2013).

[48] J. E. Peralta, J. Heyd, G. E. Scuseria, and R. L. Martin, Phys. Rev. B **74**, 073101 (2006).

[49] J. Heyd, J. E. Peralta, G. E. Scuseria, and R. L. Martin, J. Chem. Phys. **123**, 174101 (2005).

[50] P. Pernot, B. Civalleri, D. Presti, and A. Savin, J. Phys. Chem. A **119**, 5288 (2015).

[51] M. F. Peintinger, D. V. Oliveira, and T. Bredow, J. Comput. Chem. **34**, 451 (2013).

[52] A. Mascaraque, J. Avila, E. G. Michel, and M. C. Asensio, Phys. Rev. B **57**, 14758 (1998).

[53] A. Mascaraque, J. Avila, M. Asensio, and E. Michel, Surf. Sci. **433-435**, 337 (1999).

[54] A. Tejeda, R. Cortés, J. Lobo, E. G. Michel, and A. Mascaraque, J. Phys.: Condens. Matter **19**, 355008 (2007).

[55] P. Cudazzo, G. Profeta, and A. Continenza, Surf. Sci. **602**, 747 (2008).

[56] D. I. Badrtdinov, S. A. Nikolaev, M. I. Katsnelson, and V. V. Mazurenko, Phys. Rev. B **94**, 224418 (2016).

[57] J.-H. Lee, H.-J. Kim, and J.-H. Cho, Phys. Rev. Lett. **111**, 106403 (2013).

[58] J.-H. Lee, X.-Y. Ren, Y. Jia, and J.-H. Cho, Phys. Rev. B **90**, 125439 (2014).

[59] M. B. Salamon and M. Jaime, Rev. Mod. Phys. **73**, 583 (2001).

[60] G. Cao and P. Schlottmann, Rep. Prog. Phys. **81**, 042502 (2018).

[61] J. Wosnitza, J. Low Temp. Phys. **146**, 641 (2007).

[62] A. Lebed, *The Physics of Organic Superconductors and Conductors* (Springer, Berlin, 2008).

[63] E. Andrei and A. MacDonald, Nat. Mater. **19**, 1265 (2020).